



Research articles

Theoretical study of YFe_2H_x ($x = 0-5$): A comparison between cubic and orthorhombic phasesShu-Rong Yuan^a, Liuzhang Ouyang^{b,c}, Min Zhu^{b,c}, Yu-Jun Zhao^{a,b,*}^a Department of Physics, South China University of Technology, Guangzhou, Guangdong 510640, China^b Key Laboratory of Advanced Energy Storage Materials of Guangdong Province, South China University of Technology, Guangzhou, Guangdong 510640, China^c School of Materials Science and Engineering, South China University of Technology, Guangzhou, Guangdong 510640, China

ARTICLE INFO

Article history:

Received 31 October 2017

Received in revised form 9 March 2018

Accepted 15 March 2018

Available online 16 March 2018

Keywords:

First-principles calculation

Hydrogen storage

Laves phase

 YFe_2

Stability transition

ABSTRACT

The stability of binary intermetallic Laves phase YFe_2 and its hydride YFe_2H_x ($x = 0-5$) are studied using first-principles calculation. Accompanied with the analysis of the hydrogen binding energy and the formation enthalpy in various interstitial sites in YFe_2H_x , a transition of the stability from cubic to orthorhombic phase is found when hydrogen concentration increases to 1.5H/f.u. It is found that the hydrogen binding energy is very sensitive to the magnetic property of neighboring atoms. To get a further insight of the transition, we take into account external strains, as well as chemical substitution at Y site. It turns out that the transition point can be tuned by strain and chemical bonding.

© 2018 Elsevier B.V. All rights reserved.

1. Introduction

Laves phases are the largest group of intermetallic compounds, and have attracted great attentions, since Laves firstly showed us the highlights of the characteristics of this intermetallic family [1]. They are popular candidates in industrial production, especially in hydrogen energy industry, due to their unique structural, mechanical and magnetic properties [2–10]. Some particular Laves phases have high hydrogen-absorption/desorption kinetics, and considerable hydrogen storage capacity thanks to the many interstitial sites for the insertion of hydrogen [1], allowing them to be competitive hydrogen storage materials.

In spite of all these advantages Laves phases have in hydrogen storage aspect, the structural instability still places them in a dilemma about their industrial application. Laves phase AB_2 may have the structure of C15 cubic, C14 hexagonal or C36 dihexagonal type, depending on the stacking types of layers of A and B atoms [2]. The energy differences of these three types can be very small due to the close structural relation [11]. Hence, two or even three polytypes of a particular pure Laves phase can be found coexisting or transforming from one to another without much difficulty, let alone the alloy cases. Take YFe_2 , a typical ferromagnetic Laves phase, as an example. It is known to have C15 cubic structure at

normal pressure and temperature, and may transform to the hexagonal type within a high pressure [12]. Once alloyed with some particular intermetallic compounds, say YAl_2 , another C15 Laves phase, the crystal could also transform from the previous C15 cubic type to C14 hexagonal one, then back to the cubic structure, along with the addition of YAl_2 content [13–21]. When hydrogen is introduced, the lattice distortion-induced transition is reported to be more diverse and no longer limited to the cubic or hexagonal phase. Depending on the preparation conditions and the hydrogen storage amount, the cubic YFe_2 may transform into variant crystal structures after the absorption of hydrogen. $\text{YFe}_2\text{H}_{1.75}$ is found to be cubic, while $\text{YFe}_2\text{H}_{1.2}$ and $\text{YFe}_2\text{H}_{1.9}$ are reported to be tetragonal by V. Paul-boncour and co-workers [22]. $\text{YFe}_2\text{H}_{2.4}$ was found to be rhombohedral by Kanematsu [23], who also reported YFe_2H_4 to be orthorhombic [24], which, however, had been reported to be cubic by Buschow et al. earlier [25]. $\text{YFe}_2\text{H}_{2.6}$ is found to be cubic though there is local distortion [26]. $\text{YFe}_2\text{H}_{3.5}$ is reported to be monoclinic [27]. For $\text{YFe}_2\text{H}_{4.2}$, along with the increase of the temperature, a progressive transformation from monoclinic to rhombohedral and then cubic has been observed [28,29]. The saturated YFe_2H_5 is reported to have the structure of orthorhombic [30,31]. With all these different hydride phases reported by different research groups, controversies still remain about the structural stability. For a better application of YFe_2 as hydrogen storage material technically, we have to deal with this stability problem.

* Corresponding author at: South China University of Technology, Department of Physics, 381 Wushan Rd, Guangzhou, Guangdong 510640, China.

E-mail address: zhaoyj@scut.edu.cn (Y.-J. Zhao).

It would surely provide more complete information to investigate the transition with as many phases as possible considered for the overall H content range. However, there are a large amount of possible phases found experimentally for YFe₂ hydrides, like rhombohedral, tetragonal, and monoclinic. Besides, the configuration may also transform between phases along with the change of temperature. In addition, even for one specific phase, there may be structures with different space groups. Therefore, an investigation on the H-eliminated cubic and H-saturated orthorhombic phases of YFe₂H_x with variation of hydrogen concentration would present a qualitative picture of the stability transition with feasible computational efforts.

In this work, we investigate YFe₂H_x in pristine cubic phase and orthorhombic phase using first-principles calculations. It is found that the stability transition takes place around $x = 1.5$, and the hydrogen binding energy strongly depends on the magnetism of nearby host atoms. Our investigation with external pressure and chemical substitution reveals that the transition point is clearly associated with the strain and chemical bonding of the component elements.

2. Computational details

The calculations are performed based on first-principles density functional theory, as implemented in the Vienna ab initio Simulation Package [32,33]. With the use of projector-augmented wave potentials [34,35], the exchange-correlation interactions are simulated by the generalized gradient approximation using Perdew-Burke-Ernzerhof scheme [36]. The energy cutoff for the plane-wave basis set is 450 eV, except for the strain case. Hydrostatic pressure is adopted to simulate the external strain with a larger energy cutoff of 500 eV to guarantee the precision for the distortion between cubic and orthorhombic phases. The Monkhorst-Pack k-point meshes of $7 \times 7 \times 7$ and $9 \times 9 \times 7$ are used for the cubic and orthorhombic YFe₂H_x, the adopted distorted phase, respectively. For the structural optimization, all the structures in our calculations are fully relaxed until the change in the energy between two ionic steps is smaller than 1 meV.

Our analysis about the stability comparison of the two phases is mostly based on calculations of the binding energy and the formation enthalpy.

The binding energy of hydrogen is calculated by the equation

$$E_{\text{binding}} = 1/x(E_{\text{AB}_2\text{H}_x} - E_{\text{AB}_2}) - E_{\text{H}_2}/2,$$

where $E_{\text{AB}_2\text{H}_x}$ is the energy of the hydride AB₂H_x, E_{AB_2} the energy of the Laves phase AB₂, and E_{H_2} the energy of hydrogen molecule.

The formation enthalpy is calculated by the equation

$$\Delta H_{\text{formation}} = E_{\text{AB}_2\text{H}_x} - E_{\text{A}}^{\text{bulk}} - 2E_{\text{B}}^{\text{bulk}} - x\mu_{\text{H}}, \quad (1)$$

where $E_{\text{A}}^{\text{bulk}}$ and $E_{\text{B}}^{\text{bulk}}$ are the energy of A and B element in bulk phases, respectively, and the chemical potential of hydrogen μ_{H} is given respect to the H₂ molecule, i.e., $\mu_{\text{H}} = \mu_{\text{H}_2}/2 + \Delta\mu_{\text{H}}$.

3. Structure of YFe₂ and YFe₂H_x

The C15 Laves phase compound YFe₂ has a space group of *Fd-3m* with 8 yttrium atoms and 16 iron atoms locating at 8a and 16d Wyckoff site respectively in its conventional cubic cell, as shown in Fig. 1. In this unit cell, there are three types of tetrahedral interstitial sites for the insertion of hydrogen, namely A₂B₂, A₁B₃ and B₄, with the number of 96, 32 and 8, respectively. A₂B₂ tetrahedral site is also named as 96g Wyckoff site, where H atom is surrounded by 2 A atoms (here Y) and 2B atoms (here Fe). In the A₁B₃ site (or 32e site), H is surrounded by 1 A and 3B atoms. As for the B₄

site (or 8b site), H is at a regular tetrahedron with 4B atoms in the corners. Despite a totally 17 tetrahedral sites per YFe₂ formula, the experimentally reported hydrogen storage capacity of YFe₂ turns out to an extent of 5H/f.u. [37], probably due to the Switendick criterion [38], which states that the distance between H atoms should be no less than 2.1 Å. In this work, the hydrides YFe₂H_x is investigated with x ranging from 0 to 5.

To simulate the hydrides YFe₂H_x within the C15 structure, hydrogen atoms are inserted successively into the conventional cubic cell of YFe₂ until the system is saturated with H atoms. To determine the preferential absorption sites, we set the all three individual interstitials as well as the mixed cases as functions of the concentration of hydrogen for per YFe₂ formula. Taking Switendick criterion into account, we distribute these foreign atoms in a way to maximize their distance in order to minimize the repulsive interaction between them.

For the orthorhombic phase YFe₂H₅ [31], it crystallizes in the *Pmn21* space group with lattice constants of $a = 5.437$ Å, $b = 5.850$ Å, and $c = 8.083$ Å (Fig. 1). Before the dehydrogenation calculation, the magnetic property of YFe₂H₅ needs to be determined first. The stability comparison calculation between the paramagnetic and ferromagnetic orthorhombic YFe₂H₅ shows that the paramagnetic YFe₂H₅ is more stable, in agreement with the previous results. The orthorhombic YFe₂H₅ contains two kinds of inserted hydrogen, A₂B₂ and A₁B₃, with the hydrogen amount of 4/f.u. and 1/f.u., respectively. As opposed to the above cubic case where hydrogen atoms are added to the pristine C15 YFe₂, we will remove the hydrogen atoms progressively from YFe₂H₅ until the system is free of them.

4. YFe₂H_x in cubic phase

We first focus on the hydrides YFe₂H_x within the pristine C15 structure, and study about the stabilities as hydrogen inserts into three different interstitial sites. The calculated binding energy of hydrogen is shown in Fig. 2. Note that the quantities of these three kinds of sites are different from each other, so while the numbers of hydrogen atoms inserted into A₂B₂ and A₁B₃ can reach as much as 5 and 4, respectively for every YFe₂ formula, the capacity limited to B₄ sites is only 1 per YFe₂.

One may notice that the calculated binding energy is always negative, meaning a spontaneous absorption of H for the overall H content in H-rich condition. Especially, at $x = 0.5$, the H binding for B₄ case is the strongest (0.5 eV/H), avoiding the possibility of phase separation from it. The calculated zero-point energy of H at B₄ site is less than 0.2 eV, which hardly destabilizes the configuration.

Meanwhile, many previous experimental researches have observed that in the YFe₂ system, the most favorable interstitial site for hydrogen is always A₂B₂, and B₄ site absorbs least or even no hydrogen atom, which is mostly ascribed to the largest inter-space of A₂B₂ site and the smallest of B₄ [28,31,39]. From Fig. 2, however, we find that the most stable site among all the three varies along with the hydrogen concentration. At the initial stage of the hydrogen absorption process, B₄ is surprisingly found to be the most stable one, and A₂B₂ ranks the third; once the concentration of hydrogen reaches 0.75/f.u., A₁B₃ replaces B₄ to become the most favorable one; the trend changes again after 1.5H/f.u. are introduced, and only from then on does A₂B₂ become the most stable interstitial site.

We notice that all these variations of stability take place before H concentration of 1.5/f.u. Interestingly, the YFe₂ hydride with the lowest H content was reported to be YFe₂H_{1.2} experimentally. As we have considered the impact of zero-point energy and magnetic configuration (see below in this section), it leaves an open question

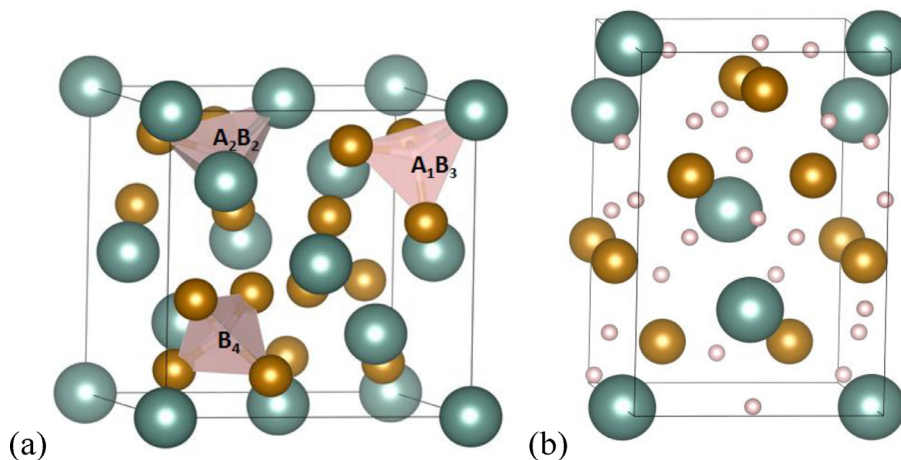


Fig. 1. Crystal structures of the cubic (a) and orthorhombic (b) phases of YFe_2H_x . Large spheres represent Y atoms, while brassy and pink ones for Fe and H, respectively. (For interpretation of the references to colour in this figure legend, the reader is referred to the web version of this article.)

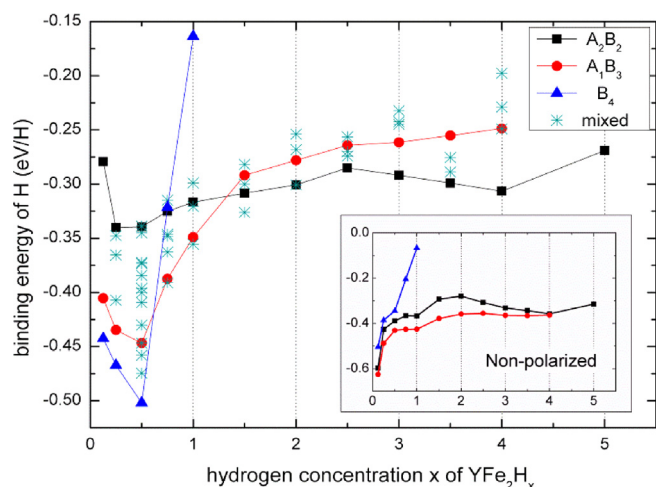


Fig. 2. Binding energy of hydrogen atom (eV/H) as a function of hydrogen concentration. The configuration of mixed A_2B_2 , A_1B_3 , and B_4 are denoted by the green asterisk. The insert figure shows the corresponding trend for the non-polarized situation. (For interpretation of the references to colour in this figure legend, the reader is referred to the web version of this article.)

whether YFe_2H_x exists for x less than 1.2, or what factor is missing in the conventional theoretical approach for this specific system.

From the theoretical point of view, once inserted into YFe_2 , hydrogen atoms attend to capture electrons from the metal atoms. By analyzing the charge transfer using Bader charge analysis, and bond length $d_{\text{Fe-H}}$ and $d_{\text{Y-H}}$ for the A_2B_2 case, we find that H captures more electrons from Fe, and is closer to Fe (1.63 Å) than Y (2.16 Å), both meaning a stronger bonding between H and Fe. As listed in Table 1, H atoms in B_4 sites obtain most electrons, combined with most electrons offered from Fe. Therefore, it is

supposed that H with larger electronegativity tends to capture electrons once inserted into the system while it is easier for Fe than Y to donate electrons to H, and thus B_4 with more Fe can provide most electrons to H atoms.

In the above discussion, all hydrogen atoms are inserted restrictedly into single kind of interstitial sites for each hydride system, which may seem to be isolated from experiment. In order to fully take into account the situation, we also consider the cases with mixed kinds of interstitial sites with the above cases, we can conclude that for YFe_2H_x restricted in cubic phase, B_4 is the most stable site to absorb hydrogen if only small amount of hydrogen is inserted; the following increasing hydrogen atoms lead to the mixed sites being the most stable; and A_2B_2 sites undoubtedly absorb most hydrogen atoms for high hydrogen concentration system.

The volume of the system is also shown in Fig. 3, from which we can find that the stability and the volume of hydrogen inserted systems are strongly associated. Hydrides with B_4 , mixed case, and A_2B_2 have the largest volume in turn along with the addition of H, which is exactly corresponding to the most energetically favored configurations. Their dominant regions also in general correspond, except for the range $x = 0.5-1$, where system of B_4 having the largest volume shows a dramatic decrease of its stability.

YFe_2 is a typical ferromagnetic Laves phase, with the magnetic moment $M = 3.26\mu_B/\text{f.u.}$ according to our calculation. With the hydrogen inserted into three different interstitial sites, its hydrides show different magnetic properties. As shown in Fig. 4, B_4 and especially A_1B_3 have generally declining magnetic moments with the addition of hydrogen apart from the very beginning stage, where all three show a slight increment. The moment of A_2B_2 has a trend of increase in a large range of region, then decreasing after more than $4\text{H}/\text{f.u.}$ are inserted.

Such a distinction may be associated with the stability differences of different interstitial sites discussed above. In order

Table 1
Charge transfer of Fe and H atoms in YFe_2H_x compared to pristine YFe_2 .

Charge transfer		$\text{YFe}_2\text{H}_{0.125}$	$\text{YFe}_2\text{H}_{0.25}$	$\text{YFe}_2\text{H}_{0.5}$	$\text{YFe}_2\text{H}_{0.75}$	YFe_2H_1
Fe	A_2B_2	-0.022	-0.048	-0.101	-0.155	-0.210
	A_1B_3	-0.025	-0.054	-0.110	-0.159	-0.220
	B_4	-0.029	-0.061	-0.128	-0.186	-0.276
H	A_2B_2	0.511	0.526	0.525	0.533	0.540
	A_1B_3	0.530	0.533	0.540	0.508	0.515
	B_4	0.574	0.580	0.608	0.569	0.614

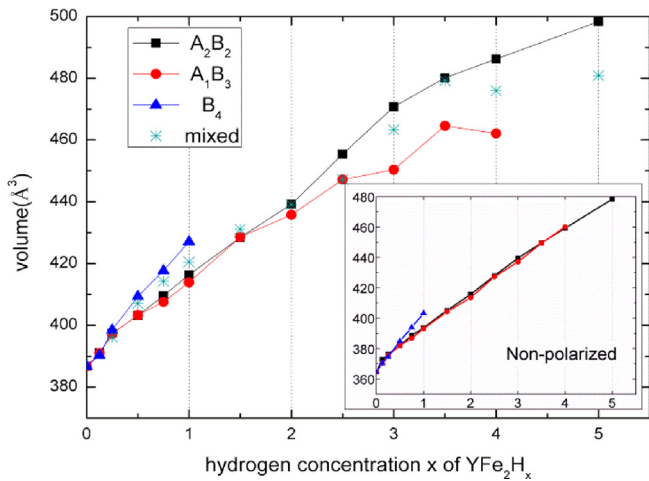


Fig. 3. Volume of YFe_2H_x with hydrogen in different interstitial sites as a function of hydrogen concentration. The insert figure shows the same relation for the non-polarized situation.

to figure out how much the magnetization counts to the properties of different sites, we consider the non-polarized case, comparing the binding energy as well as the volume to those of polarized system, as shown in the insert figures in Fig. 2 and Fig. 3, respectively. For the non-polarized YFe_2H_x , there is hardly any difference in the volumes of the three sites (c.f. insert of Fig. 3). Once the polarization is taken into consideration, hydrides of all interstitial sites expand, and the expansion seems to be proportional to the intensity of polarization. YFe_2H_x of A_2B_2 having a largest magnetic moment of all time contains a largest volume, especially in the H-rich region, while the volume expansion of A_1B_3 system that owns a smaller moment is not so obvious. The polarization also takes responsibility for the relative stability of the three. When non-polarized, the relative stability does not change of all H concentration, and A_1B_3 keeps being the most favorable one. Then the coming large magnetic moment enables A_2B_2 to be more competitive and finally become the most stable interstitial site. As for B_4 in the range of $x = 0.5\text{--}1$, for both polarized and non-polarized cases, hydrides of B_4 still has a drastic increase of binding energy while showing a largest size of volume. Therefore, as discussed above, this instability of B_4 configuration around $x = 0.5\text{--}1$ is not supposed to be directly related to the magnetization, but may be due to chemical bonding between the hydrogen and the metal atoms Fe and Y.

One may notice from Fig. 3 that the volume along with the H content obeys the Vegard's Law well in the absence of spin polarization (insert figure), which however results in a deviation once taking magnetization into account, especially in the high H concentration range for both A_2B_2 ($x > 4$) and A_1B_3 ($x > 2$) cases. We notice that the magnetization changes remarkably in that high H concentration range, as shown in Fig. 4. We take YFe_2H_2 , YFe_2H_3 and YFe_2H_5 as examples and discuss how magnetization leads the system to this deviation from the Vegard's Law.

The projected density of states (PDOS) of Fe- d orbitals is shown in Fig. 5. For YFe_2H_2 , both A_2B_2 and A_1B_3 configurations are under a considerable magnetization, and show similar PDOS. After additional 1/f.u. hydrogen is inserted, however, the magnetization of A_2B_2 clearly enhances, while the A_1B_3 one shows a drastic decrease. For A_1B_3 a large part of $d_{x^2-y^2}$ and d_{z^2} levels of the majority-spin channel turn to be unoccupied, and more d_{xy} , d_{yz} and d_{xz} levels are occupied in the minority-spin channel. Such re-distribution of the d levels leads to the decrease of the Fe magnetic moment. As for A_2B_2 , the magnetic moment of Fe also decreases when

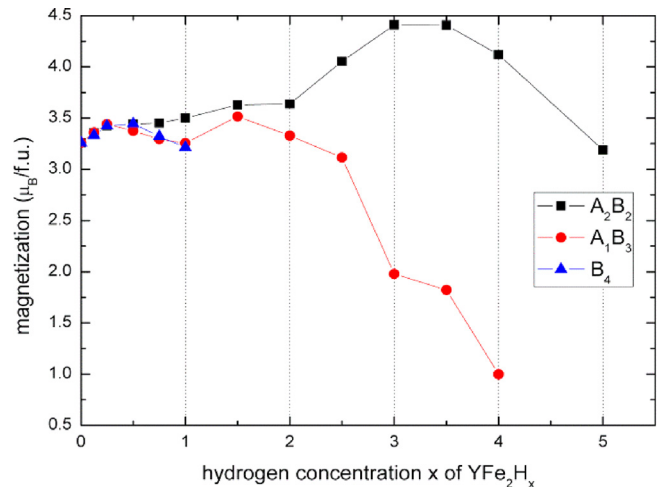


Fig. 4. Total magnetic moment of YFe_2H_x as a function of hydrogen concentration.

hydrogen concentration x goes up to 5, after the moment reaches maximum around $x = 3$. In low x ranges, we can see that the occupation of d levels changes little and thus the magnetization. When at high H concentration, the PDOS peak of the minority spin channel moves downwards and is more occupied by electrons, resulting into the decrease of Fe-moment.

The bond length change in response to spin polarization is also discussed here. The bond length between Fe and its nearest H is examined for both spin polarization and non-polarization cases for YFe_2H_2 , YFe_2H_3 and YFe_2H_5 . For hydrides of A_2B_2 , the bond length $d_{\text{Fe-H}}$ is 1.65 (1.61) Å and 1.69 (1.65) Å for polarized (non-polarized) YFe_2H_2 and YFe_2H_3 , respectively, implying that the magnetization results into an expansion of the system. For YFe_2H_5 , where magnetization has greatly decreased, things have changed. Based on different surrounding, there are two kinds of Fe sites, site 1 with fewer H neighbors still showing a certain magnetization ($2.2 \mu_B$), and site 2 with much more H neighbors obtaining Fe-moments of only $1.1 \mu_B$ in the polarized case. This tendency is in agreement with the earlier reports [37]. For Fe in site 1, the presence of polarization does lengthen $d_{\text{Fe-H}}$ from 1.63 Å to 1.70 Å. However, for Fe in site 2, the bond length $d_{\text{Fe-H}}$ of 1.64 Å keeps almost unchanged. Similar situation is also found in A_1B_3 , as in YFe_2H_2 there is obvious extension of $d_{\text{Fe-H}}$ by the introduction of spin polarization, and in YFe_2H_3 there is negligible extension for the sites with much smaller Fe-moments.

Therefore, we can conclude that spin polarization can cause volume expansion of the hydrides YFe_2H_x . As more and more H atoms are inserted, however, hydrides of both interstitials tend to show a weakening of the magnetization. The volume expansion effect would gradually vanish along with the moment reduction, which leads to a deviation from the previous trend.

To reveal the size effects of different interstitial sites due to the insertion of hydrogen, we conduct the structural optimization again, but this time with all cells keeping their original sizes and shapes, and compare the results to those obtained from the original full optimization. According to Fig. 6, we can find that the size effects of different interstitial sites show similar variation trend in general. Along with the increase of H concentration, every newly added H atom induces a larger size effect, independent of the interstitial site types, since the energy difference of the y axis in Fig. 6 is already averaged to every hydrogen atom. Specially, B_4 is mostly affected by the size effect, and that of A_1B_3 seems to be slightly less related to the volume expansion. Such differences are exactly

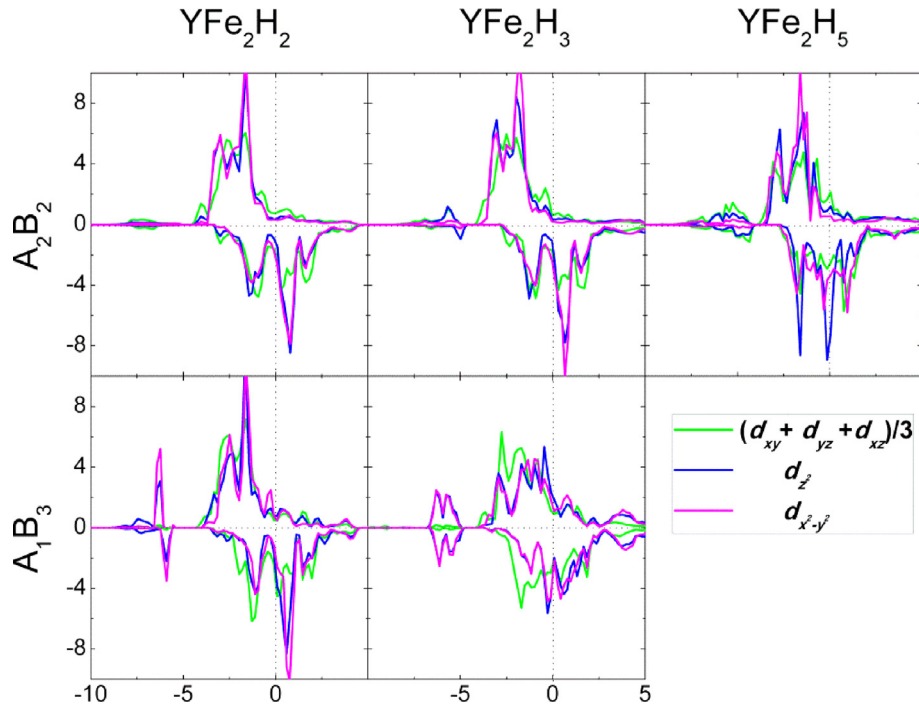


Fig. 5. Projected density of states of Fe d-levels for YFe_2H_2 , YFe_2H_3 and YFe_2H_5 . The d_{xy} , d_{yz} and d_{zx} levels are merged together as there is little difference between them. The Fermi level is set to be zero.

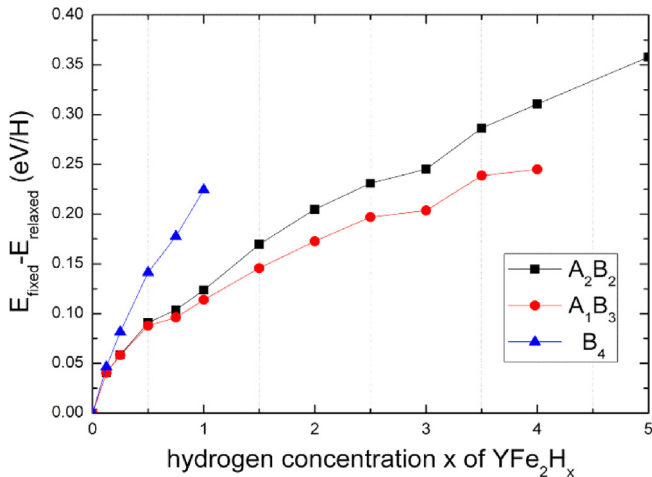


Fig. 6. Size effect to the formation enthalpy of YFe_2H_x . Here size effect is defined as the energy difference between the fully optimized structure and the corresponding structure with the original cell before H insertion.

corresponding to the volume expansion of different interstitial site shown in Fig. 3. It is reasonable as a larger expansion of the volume corresponds to a larger size effect of the inserted H atom.

5. Stability comparison between the cubic and orthorhombic phases

It is known that YFe_2 is energetically stable at cubic structure, while it prefers to orthorhombic phase when H-saturated. To figure out how the addition of hydrogen gives rise to the stability transition of YFe_2H_x from cubic to orthorhombic phase, we calculate the formation enthalpy for both phases as a function of hydrogen chemical potential. As shown in Fig. 7, under the H-poor condition, the system can hardly absorb any hydrogen atoms and prefers to

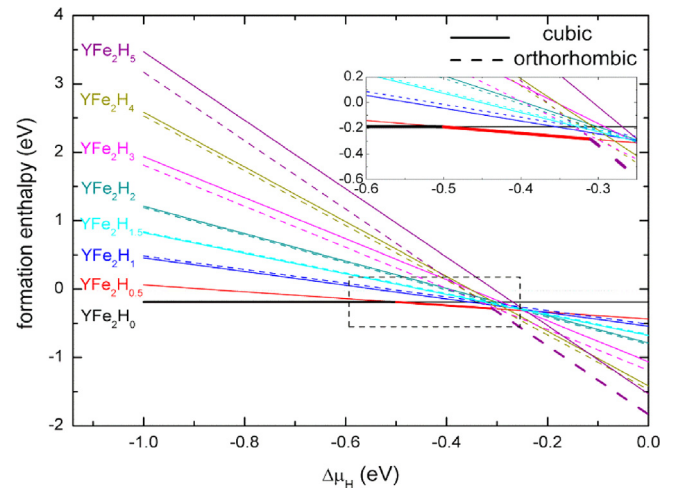


Fig. 7. Formation enthalpy of cubic and orthorhombic phases of YFe_2H_x as a function of hydrogen chemical potential.

stay in the YFe_2 state. As there comes more hydrogen, $\text{YFe}_2\text{H}_{0.5}$ becomes a new favorable state. As the environment becomes H-rich and the system absorbs more hydrogen, $\text{YFe}_2\text{H}_{0.5}$ gradually transforms to YFe_2H_5 , combined with the stability transition from cubic to orthorhombic.

As mentioned above, here in the orthorhombic case, hydrogen atoms are progressively desorbed from the reported orthorhombic YFe_2H_5 to obtain orthorhombic YFe_2H_x with all different hydrogen concentration. Of note, YFe_2H_5 contains hydrogen staying in two different interstitial sites, A_2B_2 and A_1B_3 . At the high concentration region, most hydrogen atoms prefer to stay in A_2B_2 site. However, after a large portion of hydrogen is desorbed, e.g., when only 1H/f.u. is left, all these hydrogen atoms would rather stay in A_1B_3 than in A_2B_2 , in agreement with the above cubic case. This can confirm the analysis that the stability of different interstitial sites varies along

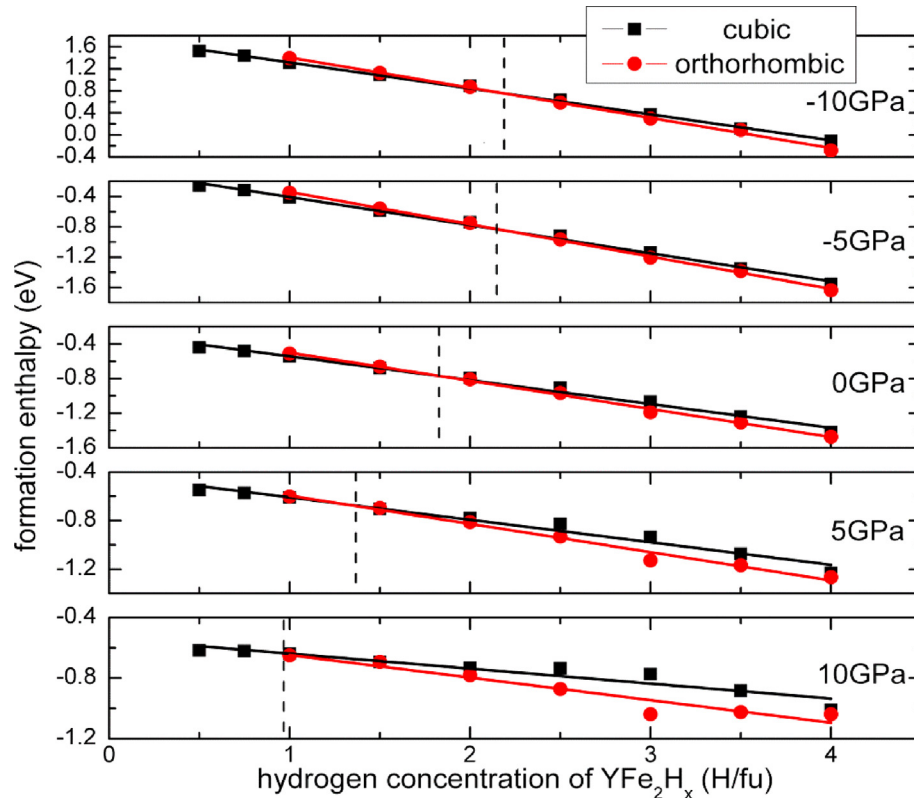


Fig. 8. Hydrogen binding energy comparison between the cubic (square, black) and orthorhombic (circle, red) phases of YFe_2 under external strain. The black dash lines denote the transition points of the stability. (For interpretation of the references to colour in this figure legend, the reader is referred to the web version of this article.)

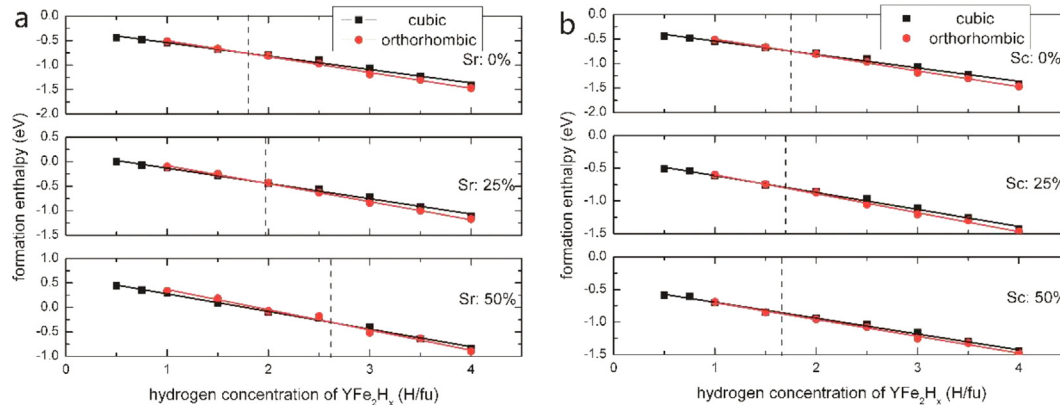


Fig. 9. Hydrogen binding energy comparison between the cubic (square, black) and orthorhombic (circle, red) phases of YFe_2 alloyed with Sr (a) and Sc (b) for different Sr or Sc concentration. The black dash lines denote the transition points. (For interpretation of the references to colour in this figure legend, the reader is referred to the web version of this article.)

with the concentration of hydrogen. We acknowledge that there is no observation of YFe_2H_x for $x < 1.2$ experimentally, which has so far not been investigated by first-principle calculations. While our calculation is not in line with the experiment observations, we think it has a stimulative effect on further investigation, either to find a way to improve the theoretical approaches, or to conduct further experimental work.

6. Tuning the transition of the stability between the two phases

According to the reported results, YFe_2 easily undergoes a phase transition with a low hydrogen concentration compared to its hydrogen capacity. It would be beneficial if we could suppress

the distortion of YFe_2 while maintaining its high hydrogen capacity. Here the influences of external strain and metal substitution on the stability transition between the cubic and orthorhombic phases are discussed.

To have a more direct impression of how the hydrogen concentration induces the stability transition and how the control measures work, we set formation enthalpy as a function of the hydrogen amount of per YFe_2 formula while keeping the hydrogen chemical potential unchanged.

6.1. External strain

We first investigate the effect of external strain to the stability transition. Hydrostatic pressure is used here to simulate the

applied strain, with magnitudes of -10, -5, 0, 5, 10 GPa, where positive ones mean external compressions and negative for tensile stresses. The stabilities comparison of the two phases is shown by the formation enthalpies, and the converted point obtained from the comparison is regarded as the transition point of the stability where the structural inclination of the system changes from cubic to orthorhombic.

A shifting trend of the location of the transition point can be seen in Fig. 8. For the original one (0 GPa), the transition of the stability occurs after 1.5H/f.u. are added. Compared with that, the system under compression tends to be orthorhombic more easily. A less amount of hydrogen can give rise to the transition of the stability, as is shown by the left shift of the transition point. A tensile stress, on the contrary, seems to help YFe_2H_x maintain its cubic structure from the effect of the inserted hydrogen. It leads to the right shift of the transition point.

The result seems to be unexpected at its first look. We know that the insertion of hydrogen results in the expansion of YFe_2 . Once the expansion is too large for the crystal to maintain its cubic phase, the distortion happens. It is therefore reasonable to believe that an external compressed stress can constrict the whole system, and hence helps maintain the original cubic structure, which, however, turns out to mismatch our calculated results.

Switendick criterion may help us interpret this strain induced shifting of the transition point. It tells us that the distance between the inserted hydrogen atoms tends to be no less than 2.1 Å so as to reduce the interaction between them. Along with the addition of hydrogen, their distance between each other will decrease. Then the stronger repulsive interaction enforces the occurrence of the transition of the stability. From this point of view, an external compression will surely further this repulsive interaction and thus prompt the transition, while a tensile strain will help to expand the system and increase the distance of the atoms. The accompanying diminished repulsive interaction will therefore postpone the transition of the stability.

6.2. Chemical doping

Next we focus on the substitution effect on the transition of the stability. YFe_2 alloyed with ZrFe_2 , or $\text{Y}_{1-x}\text{Zr}_x\text{Fe}_2$, has been studied and shown to effectively stabilize the cubic structure [24,40]. However, since ZrFe_2 can hardly absorb hydrogen spontaneously [41], the higher the concentration of Zr, the smaller the capacity of hydrogen. Further research is necessary about the use of YFe_2 alloyed with ZrFe_2 . Here we choose Strontium and Scandium, two other neighbor metal elements of yttrium, as substitutions. Two concentrations, 25% and 50%, are adopted to examine how the transition point of the stability shifts along with the introduction of Sr or Sc.

As is shown in Fig. 9, the two substitution species affect differently to the transition of the stability. For the original YFe_2H_x , the transition takes place after absorbing 1.5/f.u. hydrogen. After 25% Sr is introduced, the transition point shifts toward the high H-concentration side. As for the higher Sr-concentration system $\text{Y}_{0.5}\text{Sr}_{0.5}\text{Fe}_2\text{H}_x$, the crystal keeps its cubic structure unchanged until more than 2.5/f.u. of hydrogen is absorbed. The introduction of Sr helps YFe_2H_x keep the cubic structure. The introduction of Sc, however, can barely influence the transition of the YFe_2 . The stability transition keeps always unchanged for all different Sc content.

Combining the already reported Zr result [24,40], a little of which can keep the crystal structure maintaining C15 type, we can find that it is the electronic structure instead of the size effect that counts the most here in the substitution case. Although the substitution of Sr may destabilizes the whole system as is shown by the positive formation enthalpy in Fig. 9(a), Sr and Zr, having different numbers of valence electrons from Y, can lead to a post-

ponement of the transition of the stability, despite that Zr has a smaller ionic radius than Y and Sr larger. Sc, which has a smaller ionic radius but the same valence electrons number with Y, turns out to do little to the transition.

7. Conclusions

The transition of the stability of YFe_2H_x from cubic to orthorhombic phase is studied by first-principles calculations to present a qualitative picture of the transition of YFe_2H_x as x increase. It is found that hydrogen atoms favor different interstitial sites at different concentration. The stability transition from cubic to orthorhombic phase is found to take place around $x = 1.5$, a relative small value compared to the hydrogen capacity of YFe_2 . It is found that the magnetism plays an important role in the hydrogen adsorption. Furthermore, it is found that external tensile strains could maintain its cubic phase to a higher hydrogen concentration. Meanwhile, the transition point is mainly due to the chemical bonding rather than the size effect of the substitutional metals.

Acknowledgments

This work is financially supported by NSFC (Grant Nos. 11574088 and 51431001), the Foundation for Innovative Research Groups of the National Natural Science Foundation of China (Grant No. 51621001), and Natural Science Foundation of Guangdong Province of China (Grant No. 2016A030312011).

References

- [1] S.F. Matar, *Intermetallic hydrides: a review with ab initio aspects*, *Prog. Solid State Chem.* 38 (2010) 1–37.
- [2] F. Stein, M. Palm, G. Sauthoff, Structure and stability of Laves phases. Part I. Critical assessment of factors controlling Laves phase stability, *Intermat*, 12 (2004) 713–720.
- [3] J.J. Didisheim, K. Yvon, D. Shaltiel, The distribution of the deuterium atoms in the deuterated hexagonal Laves-phase ZrMn_2D_3 , *Solid State Commun.* 31 (1979) 47–50.
- [4] J.J. Didisheim, K. Yvon, Order-disorder phase transition in $\text{ZrV}_2\text{D}_{3,6}$, *Solid State Commun.* 38 (1981) 637–641.
- [5] S. Hong, C.L. Fu, Hydrogen in Laves phase ZrX_2 (X=V, Cr, Mn, Fe Co, Ni) compounds: Binding energies and electronic and magnetic structure, *Phys. Rev. B* 66 (2002) 094109.
- [6] R.Z. Huang, Y.M. Wang, J.Y. Wang, Y.C. Zhou, First-principles investigations of the stability and electronic structure of ZrV_2H_x ($x=0.5, 1, 2, 3, 4, 6$ and 7), *Acta Mater.* 52 (2004) 3499–3506.
- [7] W.Y. Yu, N. Wang, X.B. Xiao, B.Y. Tang, L.M. Peng, W.J. Ding, First-principles investigation of the binary AB_2 type Laves phase in Mg–Al–Ca alloy: electronic structure and elastic properties, *Solid State Sci.* 11 (2009) 1400–1407.
- [8] J. Radaković, J. Belošević-Cavor, V. Koteski, Hydrogen storage in Laves phases: First principles study of electronic structure and formation energies in HV₂ hydrides, *Int. J. Hydrogen Energy* 38 (2013) 9229–9235.
- [9] A.R. Merlini, C.R. Luna, A. Juan, M.E. Pronato, A DFT study of hydrogen storage in $\text{Zr}(\text{Cr}_{0.5}\text{Ni}_{0.5})_2$ Laves phase, *Int. J. Hydrogen Energy* 41 (2016) 2700–2710.
- [10] V. Paul-Boncour, S.M. Filipek, M. Dorogova, F. Bourée, G. André, I. Marchuk, A. Percheron-Guégan, R.S. Liu, Neutron diffraction study, magnetic properties and thermal stability of YMn_2D_3 synthesized under high deuterium pressure, *J. Solid State Chem.* 178 (2005) 356–362.
- [11] F. Stein, Consequences of crystal structure differences between C14, C15, and C36 Laves phase polytypes for their coexistence in transition-metal-based systems, *Mater. Res. Soc. Symp. Proc.* 1295 (2011).
- [12] F. Stein, M. Palm, G. Sauthoff, Structure and stability of Laves phases part II—structure type variations in binary and ternary systems, *Intermat* 13 (2005) 1056–1074.
- [13] K.H.J. Buschow, Crystal structure and magnetic properties of $\text{YFe}_2\text{Al}_{2-x}$ compounds, *J. Less-Common Met.* 40 (1975) 361–363.
- [14] Y. Muraoka, M. Shiga, Y. Nakamura, Magnetic properties and Mössbauer effect of $\text{A}(\text{Fe}_{1-x}\text{B}_x)_2$ (A = Y or Zr, B = Al or Ni) Laves phase intermetallic compounds, *Phys. Stat. Sol.* 42 (1977) 369–374.
- [15] H. Oesterreicher, Magnetic properties of scatter order compounds RFeAl (R = Gd, Tb, Dy, Ho, Er, Tm, Lu, and Y), *Phys. Stat. Sol.* 40 (1977) K139–K143.
- [16] M.J. Besnus, P. Bauer, J.M. Génin, Magnetic and ^{57}Fe Mössbauer study of $\text{Y}(\text{Fe}_{1-x}\text{Al}_x)_2$ alloys: Local environment effects, *J. Phys. F: Met. Phys.* 8 (1978) 191–204.
- [17] W. Steiner, Magnetization processes caused by iron substitution in cubic Laves phases, *J. Magn. Magn. Mater.* 14 (1979) 47–79.

- [18] M. Reissner, W. Steiner, J.P. Kappler, P. Bauer, M.J. Besnus, Magnetic behaviour of $\text{Y}(\text{Fe}_x\text{Al}_{1-x})_2$ alloys, *J. Phys. F: Met. Phys.* 14 (1984) 1249–1259.
- [19] M. Aoki, H. Yamada, Isomer shift and atomic environment effect in the intermetallic compound $\text{Y}(\text{Fe}_{1-x}\text{Al}_x)_2$, *J. Magn. Magn. Mater.* 104–107 (1992) 1965–1966.
- [20] M.T.F. Telling, J.A. Dann, R. Cywinski, J. Bogner, M. Reissner, W. Steiner, Spin dynamics in the concentrated spin-glass system $\text{Y}(\text{Al}_{1-x}\text{Fe}_x)_2$, *Phys. B* 289–290 (2000) 213–216.
- [21] J.M. Preston, J.R. Stewart, M. Reissner, W. Steiner, R. Cywinski, A neutron polarisation analysis study of the spin-glass phase of $\text{Y}(\text{Al}_{1-x}\text{Fe}_x)_2$, *Appl. Phys. A: Mater. Sci. Process* 74 (2002) S689–S691.
- [22] V. Paul-Boncour, M. Latroche, L. Guénee, A. Percheron-Guégan, Multiphase isotherms related to a multiphase behaviour in the $\text{YFe}_2\text{-D}_2$ system, *J. Alloys Compd.* 255 (1997) 195–202.
- [23] K. Kanematsu, Ferromagnetism of YFe_2H_x , *J. Appl. Phys.* 75 (1994) 7105–7107.
- [24] K. Itoh, K. Kanematsu, Mössbauer studies on the hydrogenation effect in ferromagnetic C15-type compounds $\text{Y}_{1-x}\text{Zr}_x\text{Fe}_2$, *J. Magn. Magn. Mater.* 104–107 (1992) 1279–1280.
- [25] K.H.J. Buschow, A.M.v. Diepen, Effect of hydrogen absorption on the magnetic properties of YFe_2 and GdFe_2 , *Solid State Commun.* 19 (1976) 79–81.
- [26] A.V. Skripov, V. Paul-Boncour, T.J. Udovic, J.J. Rush, Hydrogen dynamics in Laves-phase hydride $\text{YFe}_2\text{H}_{2.6}$: Inelastic and quasielastic neutron scattering studies, *J. Alloys Compd.* 595 (2014) 28–32.
- [27] G. Wiesinger, V. Paul-Boncour, S.M. Filipek, C. Reichl, I. Marchuk, A. Percheron-Guégan, Structural and magnetic properties of RFe_2D_x deuterides ($\text{R} = \text{Zr}, \text{Y}$ and $x \geq 3.5$) studied by means of neutron diffraction and ^{57}Fe Mössbauer spectroscopy, *J. Phys.: Condens. Matter* 17 (2005) 893–908.
- [28] V. Paul-Boncour, M. Guillot, G. André, F. Bourée, G. Wiesinger, A. Percheron-Guégan, Origin of the first order magnetostructural transition in $\text{YFe}_2\text{D}_{4.2}$, *J. Alloys Compd.* 404–406 (2005) 355–359.
- [29] J. Ropka, R. Černý, V. Paul-Boncour, T. Proffen, Deuterium ordering in Laves-phase deuteride $\text{YFe}_2\text{D}_{4.2}$, *J. Solid State Chem.* 182 (2009) 1907–1912.
- [30] V. Paul-Boncour, S.M. Filipek, A. Percheron-Guégan, I. Marchuk, J. Pielaszek, Structural and magnetic properties of RFe_2H_5 hydrides ($\text{R} = \text{Y}, \text{Er}$), *J. Alloys Compd.* 317–318 (2001) 83–87.
- [31] V. Paul-Boncour, S.F. Matar, Ab initio approach of the hydrogen insertion effect on the magnetic properties of YFe_2 , *Phys. Rev. B* 70 (2004).
- [32] G. Kresse, J. Furthmüller, Efficiency of ab-initio total energy calculations for metals and semiconductors using a plane-wave basis set, *Comput. Mater. Sci.* 6 (1996) 15–50.
- [33] G. Kresse, J. Furthmüller, Efficient iterative schemes for ab initio total-energy calculations using a plane-wave basis set, *Phys. Rev. B* 54 (1996) 11169–11186.
- [34] P.E. Blöchl, Projector augmented-wave method, *Phys. Rev. B* 50 (1994) 17953–17979.
- [35] G. Kresse, D. Joubert, From ultrasoft pseudopotentials to the projector augmented-wave method, *Phys. Rev. B* 59 (1999) 1758–1775.
- [36] J.P. Perdew, K. Burke, M. Ernzerhof, Generalized gradient approximation made simple, *Phys. Rev. L.* 77 (1996) 3865–3868.
- [37] V. Paul-Boncour, M. Guillot, O. Isnard, B. Ouladdiaf, A. Hoser, T. Hansen, N. Stuesser, Interplay between crystal and magnetic structures in $\text{YFe}_2(\text{H}_2\text{D}_{1-x})_{4.2}$ compounds studied by neutron diffraction, *J. Solid State Chem.* 245 (2017) 98–109.
- [38] A.C. Switendick, Band structure calculations for metal hydrogen systems, *Z. Phys. Chem. Neue Folge* 117 (1979) 89–112.
- [39] M. Latroche, V. Paul-Boncour, A. Percheron-Guégan, F. Bourée-Vigneron, Crystallographic study of $\text{YFe}_2\text{D}_{3.5}$ by X-ray and neutron powder diffraction, *J. Solid State Chem.* 133 (1997) 568–571.
- [40] K.K.K. Kobayashi, Magnetic properties and crystal structure of laves phase $(\text{Y}_x\text{Zr}_{1-x})\text{Fe}_2$ and their hydrides, *J. Phys. Soc. Jpn.* 55 (1986) 1336–1340.
- [41] L. Rabahi, M. Gallouze, T. Grosdidier, D. Bradai, A. Kellou, Energetics of atomic hydrogen absorption in C15- Fe_2Zr Laves phases with ternary additions: A DFT study, *Int. J. Hydrogen Energy* 42 (2017) 2157–2166.